Plasma Physics and Controlled Fusion

PAPER

# Co- and counter-current rotation in Tore Supra lower hybrid current drive plasmas

To cite this article: B Chouli *et al* 2014 *Plasma Phys. Control. Fusion* **56** 095018

IOP Publishing

Plasma Physics and Controlled Fusion

Plasma Phys. Control. Fusion **56** (2014) 095018 (8pp)

doi:10.1088/0741-3335/56/9/095018

# Co- and counter-current rotation in Tore Supra lower hybrid current drive plasmas

**B Chouli, C Fenzi, X Garbet, C Bourdelle, J Decker, T Aniel, J-F Artaud, V Basiuk, F Clairet, G Colledani, R Dumont, D Elbeze, C Gil, P Lotte, Y Sarazin, and the Tore Supra Team**

CEA, IRFM, F-13108 St Paul-lez-Durance, France

E-mail: billal.chouli@cea.fr

Received 5 March 2014, revised 20 June 2014
Accepted for publication 30 June 2014
Published 30 July 2014

**Abstract**

Observations of lower hybrid (LH) radio frequency heating effects on toroidal plasma rotation in L-mode Tore Supra plasmas are reported. A database of more than 50 plasma discharges has been analysed. Core rotation is found to increment in co- or counter-current direction depending on the plasma current ($I_p$). At low plasma current, the induced rotation is up to $+15\,\mathrm{km\,s^{-1}}$ in the co-current direction, the rotation profile being affected over the whole plasma minor radius. At higher plasma current, an opposite trend is observed, the core plasma rotation incrementing up to $-15\,\mathrm{km\,s^{-1}}$ in the counter-current direction, the profile being affected up to $r/a < 0.6$ only. At the zero crossing point, which is defined when the plasma rotation profile is not affected by LH power injection, $I_p \sim 0.95\,\mathrm{MA}$. In both low and high $I_p$ cases, rotation increments are found to increase with the injected power. Several mechanisms in competition which can induce co- or counter-current rotation in Tore Supra LHCD plasmas are investigated and typical order of magnitude are discussed. How those effects evolve with plasma parameters and how they compete are important issues addressed in this paper. Rotation increment increase with $I_p$ at fixed LH power is consistent with a dominant standard momentum confinement mechanism related to $I_p$ increase. The co-current change in rotation is consistent with a fast electron ripple loss mechanism, while thermal ripple induced neoclassical friction and absorbed LH wave momentum from resonant electrons are expected to influence the rotation in the counter-current direction. Finally, the numerical simulations show that the radial turbulent momentum transport does impact the rotation behaviour inducing increment in co- or counter-current directions, depending on the plasma current amplitude.

Keywords: intrinsic toroidal rotation, LHCD induced rotation, fast electron effect, toroidal momentum transport, Laplace force, neoclassical friction

(Some figures may appear in colour only in the online journal)

## 1. Introduction

Plasma rotation in tokamaks has been an area of active interest in the past few years, due to its impact onto magnetohydrodynamics (MHD) stability, transport and plasma performance. In particular, when the rotation is associated with a sufficiently large $E \times B$ shear, it can stabilize turbulence [1], leading to enhanced energy and particle confinement as observed in plasmas with transport barriers. Also, large enough toroidal rotation may help to stabilize resistive wall mode instabilities [2]. In present fusion devices, strong plasma rotation is often provided by neutral beam injection (NBI) which provides a significant external momentum source. However, NBI induced torque is expected to be low in ITER [3], partly due to the high injection energy $E_{\mathrm{inj}}$ required since the ratio $P_{\mathrm{NBI}}/V_{\mathrm{olume}}$ is low. Hence, exploring the mechanisms underlying 'intrinsic rotation', i.e. plasma rotation that develops in the absence of any externally applied torque, is of prime interest in order to improve our predictions for plasma rotation in ITER and future machines.

 

Intrinsic plasma rotation can be understood as resulting from the competition between several effects: MHD effects [4], turbulent transport processes, fast particle effects [5] and 3D effects such as those induced by resonant magnetic field perturbations or ripple [6]. The latter arises from the variation in toroidal magnetic field (TF) magnitude due to the finite number of TF coils, hence it is present in all tokamak devices. The relative amplitude of ripple reads $\delta = (B_{\max} - B_{\min}) / (B_{\max} + B_{\min})$ where $B_{\max}$ is the TF under the TF coil and $B_{\min}$ is the TF between two coils. It breaks the magnetic field axisymmetry, enhances particle losses, and induces non-ambipolar particle fluxes. Those fluxes are source of momentum and might influence the plasma rotation. More precisely, friction on trapped particles in banana orbits and in ripple wells [7] leads to toroidal flows generation, affecting the toroidal plasma rotation. How those effects evolve with plasma parameters such as the plasma current or the radio frequency injected power for instance, and how they compete with fast particles generation and turbulent transport processes are important issues to address in order to better understand the behaviour of intrinsic rotation.

In this paper, we will focus on plasma rotation behaviour with lower hybrid radio frequency (LHRF) power. LH-driven rotation has been reported so far in C-Mod [8–11], EAST [12], JET [13], JT60U [14] and Tore Supra [15, 16]. Co-current increments of rotation have been observed in most of those devices, but in C-Mod where both co- and counter-rotation increments have been reported. Interestingly, counter-current rotation increments has been found to occur in high plasma current configuration only, above an $I_p$ threshold $I_{p,\text{threshold}} = 0.4 - 0.6$ MA depending on the magnetic configuration (lower single null versus upper single null) [8]. Recent dedicated experiments have been performed in Tore Supra, aiming at clarifying intrinsic rotation behaviour at low and high plasma currents and better understand the various mechanisms at play. Tore Supra is a well suited device to address those issues, with a LHRF power capability up to 5 MW and no external momentum input from NBI. More than 50 plasma discharges have been analysed, with lower hybrid (LH) power $P_{LH}$ up to 4.8 MW, plasma current $I_p$ up to 1.4 MA, line integrated density $n_l$ up to $6 \times 10^{19}\,\text{m}^{-2}$, and a significant ripple amplitude (up to 5% at the plasma boundary) which makes ripple-induced momentum non-negligible. This paper is organized as follows: after a description of the experimental setup in section 2, experimental results are reported in section 3. In order to explain the LH power injection effects, an important theoretical effort has been made. Experimental results, interpretation and discussion on the contributions of the various potential mechanisms impacting on toroidal momentum balance equation (ripple, turbulence, fast electrons and LH wave effects) are given in section 4. Finally, a summary and a conclusion are given in section 5.

## 2. Experimental setup

Tore Supra is a large tokamak, with a major radius of $R = 2.4$ m and a minor radius of $a = 0.7$ m. The machine is equipped with 18 superconducting coils, allowing for a magnetic field up to 4.2 T and long pulse operation. The ripple amplitude is strong, around 5% at the plasma boundary (figure 1) under standard plasma conditions in contrast to JET ripple strength (∼0.3%) and expected ripple in ITER (about 0.5%). The plasmas to be discussed have been performed in L-mode, limiter configuration, at a magnetic field $B_T = 3.8$ T and plasma current $I_p = 0.6 - 1.22$ MA (both directed clockwise), $P_{LH} = 1 - 4.8$ MW and $n_l = 3.8 - 6 \times 10^{19}\,\text{m}^{-2}$. Electron temperature profiles are determined from electron cyclotron emission (ECE) and Thomson scattering measurements [17], electron density profiles are provided using interferometry and reflectomety techniques [18, 19] and ripple loss information is provided by a ripple dedicated diagnostic 'DRIPPLE' [20]. Plasma current density and $q$-profiles are obtained from EFIT (using polarimetry measurements as a constraint) and CRONOS [21] simulations, the edge safety factor ($q_a$) ranging from 2.5 to 8. Rotation profiles are provided with charge exchange recombination spectroscopy measurements (CXRS) [22], using diagnostic neutral beam injection (DNBI). The system provides measurements of ion temperature ($T_i$) and plasma toroidal rotation velocity ($V_\varphi$) profiles, as well as ion density ($n_i$) profiles from carbon line (C VI line at 5290 Å) spectral line analysis, assuming that the carbon impurity has the same velocity and temperature as the main plasma impurity [23, 24]. Fifteen tangential viewing lines are used (figure 1), allowing for a spatial coverage from the plasma core to $r/a = 0.9$ normalized minor radius in the equatorial plane, with 2 cm spatial resolution at the plasma edge and 6 cm in the core [19]. The time resolution is set at 10–50 ms, in order to improve signal to noise ratio depending on the plasma conditions. The DNBI system provides short and low power beam pulses (deuterium beam, 300 ms pulse, injected energy $E_{inj} = 60$ keV, injected power $P_{DNBI} = 400$ kW, nearly perpendicular injection), the momentum carried out by the injected particles being expected to be low. A laser at 5320.43 Å wavelength is used as a reference line for Doppler shift calculations in order to get accurate $V_\varphi$ measurements. To deal with the complex measured spectra, a multi-Gaussian fit software (CXSFIT) is used [25]. Each spectrum consists of passive and active component combination as shown in

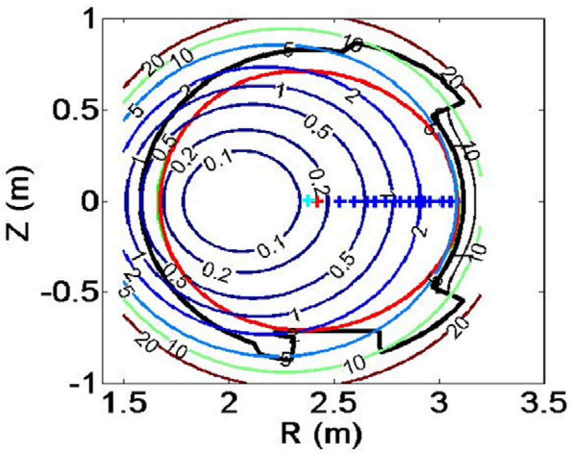


**Figure 1.** Poloidal section of Tore Supra showing the iso-amplitude ripple contours (%) and CXRS measurement locations (crosses).

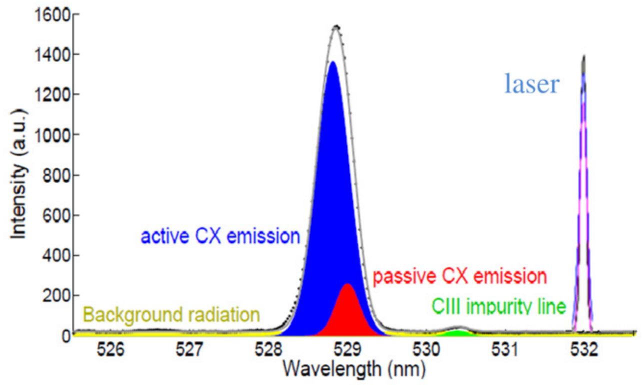


**Figure 2.** Typical CXSFIT spectrum. The solid grey line is the result of a fitting routine. The different components of the CX spectrum are indicated: the active CX in blue, the passive CX in red, a C III impurity line in green and the background radiation is yellow. The laser ($\lambda \sim 5320.43$) used as a reference line is shown in blue.

figure 2. The former component is mainly due to low ionization stage radiation emission from a narrow plasma layer close to the plasma boundary. The active component is due to local emission from the so-called 'active volume', which is defined by the intersection of the neutral beam and the viewing-line path, hence allowing for spatially resolved measurements. For the measurements to be discussed here, statistical errors of less than 1 km s$^{-1}$ for $V_\varphi$ and less than 50 eV for $T_\mathrm{i}$ were obtained.

The LH heating system of Tore Supra consists of two types of launchers with passive active multijunction (PAM) [26] and full active multijunction (FAM) units [27]. PAM units consist of sixteen modules, each module comprising six active waveguides and six passive waveguides, while FAM units consist of sixteen 500 kW klystrons. The two launchers are actively cooled in order to be able to operate in long pulse configuration, up to 1000 s (low power operation). The maximum power expected to be coupled to the plasma with the present system is in the range of 5–6 MW (short plasma discharges). LH waves are launched into the plasma with a parallel refractive index $n_\parallel = ck_\parallel/\omega$ between 1.5 and 3.2. Expected wave-induced momentum input is in the counter-current direction (the electrons being accelerated). The LH power deposition is off-axis, with a maximum deposition at $r/a \sim 0.3$, then decreasing towards the edge with a minimum power deposition at $r/a \sim 0.7$ as illustrated in figure 3 showing typical hard x-ray emission profiles at different plasma currents. As usually observed in Tore Supra, the deposition profiles broaden and the maximum deposition location is shifted outwards when the plasma current increases [28, 29].

## 3. Experimental results

The plasma rotation behaviour is investigated in two sets of lower hybrid current drive (LHCD) plasma discharges, at high (1.2 MA) resp. low (0.7 MA) plasma currents, $n_\mathrm{l} = 5.3 - 5.9 \times 10^{19}\,\mathrm{m}^{-2}$ resp. $n_\mathrm{l} = 3.5 - 3.9 \times 10^{19}\,\mathrm{m}^{-2}$, $P_\mathrm{LH} = 1 - 4.8$ MW, $n_\parallel \sim 1.8$ (maximum $n_\parallel$ of the primary lobe in the parallel refractive index spectrum). Ohmic (OH) plasmas with similar plasma parameters are also considered and used as reference plasmas.

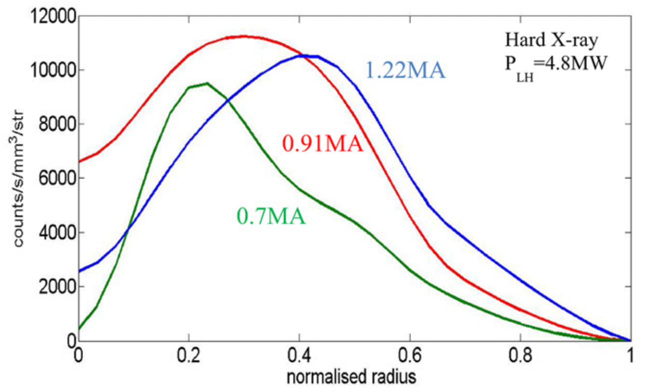


**Figure 3.** Hard x-ray absorption profiles for three LHCD discharges at $P_\mathrm{LH} = 4.8$ MW with different plasma current. For higher $I_\mathrm{p}$ the profile deposition is broader and outermost.

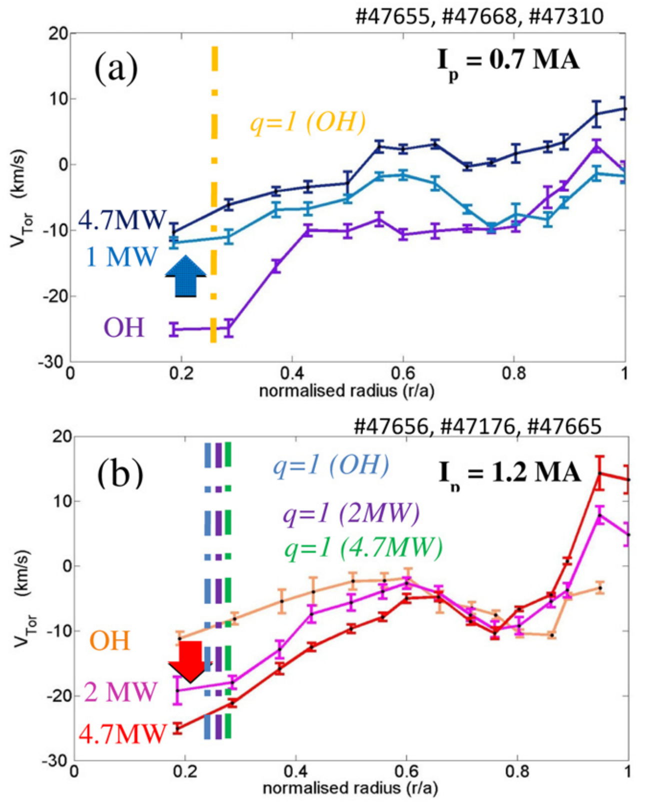


**Figure 4.** Toroidal rotation profile modifications between OH and LHCD plasmas, at low $I_\mathrm{p} = 0.7$ MA($a$) and high plasma current $I_\mathrm{p} = 1.2$ MA($b$). The $q = 1$ surface locations are also indicated.

In LHCD plasmas, significant increments of plasma toroidal rotation are observed in the co- or counter-current direction, depending on the plasma current amplitude as illustrated in figure 4. The LH power effect is confirmed and remains strong when considering the total angular momentum $L$ evolution with $P_\mathrm{LH}$, reading as $L \sim m_\mathrm{i} n_\mathrm{i} < R^2 > V_\varphi/R$ (where $m_\mathrm{i}$ is the impurity mass, $R$ is the plasma major radius and brackets indicate flux average), shown in figure 5. The precedent approximation of the total angular momentum $L$,

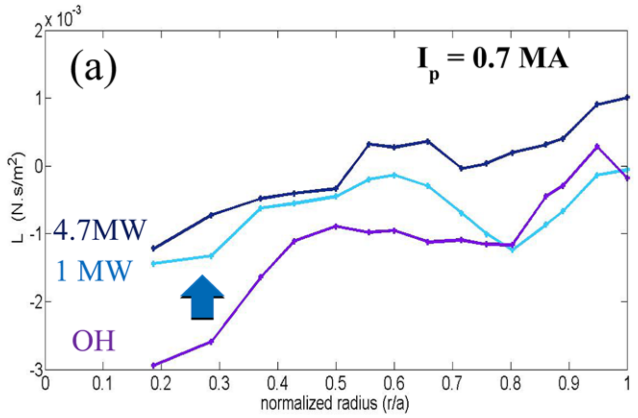


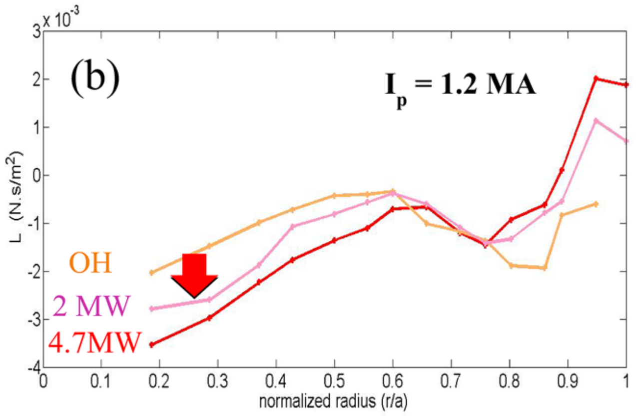


**Figure 5.** Toroidal angular momentum profile modifications between OH and LHCD plasmas, at low $I_p = 0.7$ MA (*a*) and high plasma current $I_p = 1.2$ MA (*b*). Similar trends are observed compared to the rotation profiles.

derives from $L = m_i n_i < RV_\varphi^q >$. Assuming that $V_\varphi^q = \omega_\varphi R + u_\theta F/R$ where $\omega_\varphi$ is the toroidal angular frequency, $u_\theta$ the poloidal velocity, $F$ is the diamagnetic function and $q$ refers to the flux surface, neglecting the poloidal velocity and taking $\omega_\varphi = V_\varphi/R$, one can obtain that $L \sim m_i n_i < R^2 > V_\varphi/R$ [21].

At low plasma current (0.7 MA), a co-current increment is observed (figures 4(*a*) and 5(*a*)), increasing with the injected LH power. Also, it is worth mentioning that the effect is visible across the whole plasma minor radius, with a maximum increment of about $+15\,\mathrm{km\,s^{-1}}$ in the core plasma region ($r/a < 0.35$). One can also notice that the plasma core velocity remains in the counter-current direction, while the edge plasma rotation ($r/a > 0.8$) becomes co-current in the highest power case. There is no sawtooth activity in this set of LHCD plasma discharges (according to ECE measurements), and the $q$-profiles are slightly reversed in the plasma core with $q_0$ above 1, according to CRONOS simulations obtained by resolving the current diffusion equation including the current sources and the resistivity (figure 6). EFIT $q$-profiles (constrained by IR-polarimetry), illustrated in figure 6, are consistent with CRONOS simulations except for low plasma current case where the reversal was not reproduced. Note, however that for the OH plasma used as reference, a sawtooth activity is observed with a sawtooth period of about 30 ms and the surface $q = 1$ being located at $R \sim 2.6$ m ($r/a \sim 0.25 - 0.3$).

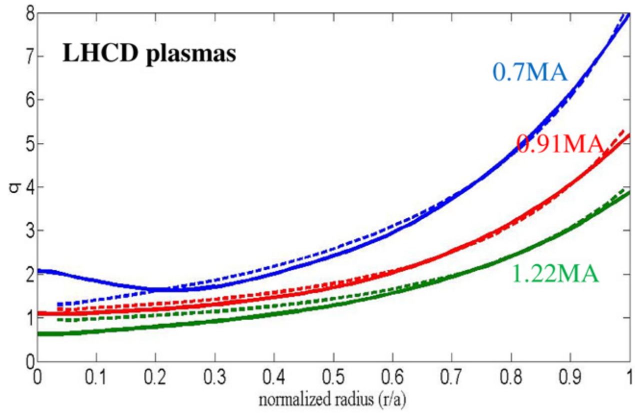


**Figure 6.** $q$-profiles from CRONOS current diffusion simulations (solid curves) and EFIT (dashes curves) for high, intermediate and low plasma current discharges during the LHCD phase.

At high plasma current (1.2 MA), an opposite trend is observed. The core plasma rotation increment is in the counter-current direction with a maximum effect of about $-15\,\mathrm{km\,s^{-1}}$ (Figures 4(*b*) and 5(*b*)) in the highest LH power plasma. It is worth pointing out in this case that the profile remains unaffected for $0.6 < r/a < 0.9$. However at the very plasma edge ($r/a > 0.9$), the velocity increases in the co-current direction with the LH power (similar trend observed in the low plasma current case), which could be consistent with the existence of a secondary lobe (in the opposite direction comparing to the primary lobe) in the parallel refractive index spectrum, which would directly transfer momentum to electrons at the plasma edge and could induce co-current rotation as indicated by LUKE simulations [30]. Finally, sawteeth are observed in this set of high plasma current discharges (transition phase in the highest LH power plasma), and the related $q$-profiles (EFIT and CRONOS) are monotonic with $q_0$ slightly below 1 (figure 6). The sawtooth period is about 50 ms and the surface $q = 1$ being located between $r/a \sim 0.25$ and 0.3. The rotation measurements are realized after the sawtooth crash for the two sets of plasmas.

Further information on plasma rotation behaviour can also be obtained comparing an additional set of plasma discharges in LHCD scenario with similar LH power and $n_l$, but different $I_p$ amplitudes (figure 7). In the present LHCD plasmas (fixed $P_{LH}$), LH waves induced momentum and fast electron ripple loss effect add to the turbulence driven mechanisms and thermal ripple induced effects, already present in OH plasmas. The rotation profiles are in the counter-current direction over the whole plasma radius (figure 7(*a*)). The rotation ($|V_\varphi|$) increases with $I_p$ in the bulk plasma region up to $r/a < 0.8$, with a maximum increment of about $-15\,\mathrm{km\,s^{-1}}$ in the core. The discharges used here, present a slight density variation, nevertheless the impact of the plasma current amplitude is corroborated when considering the total angular momentum $T$ evolution with the plasma current effect, as illustrated in figure 7(*b*).

In order to investigate further such a dual effect of LH injection power on plasma rotation, one can focus on the core plasma rotation ($r/a < 0.35$) behaviour at different plasma

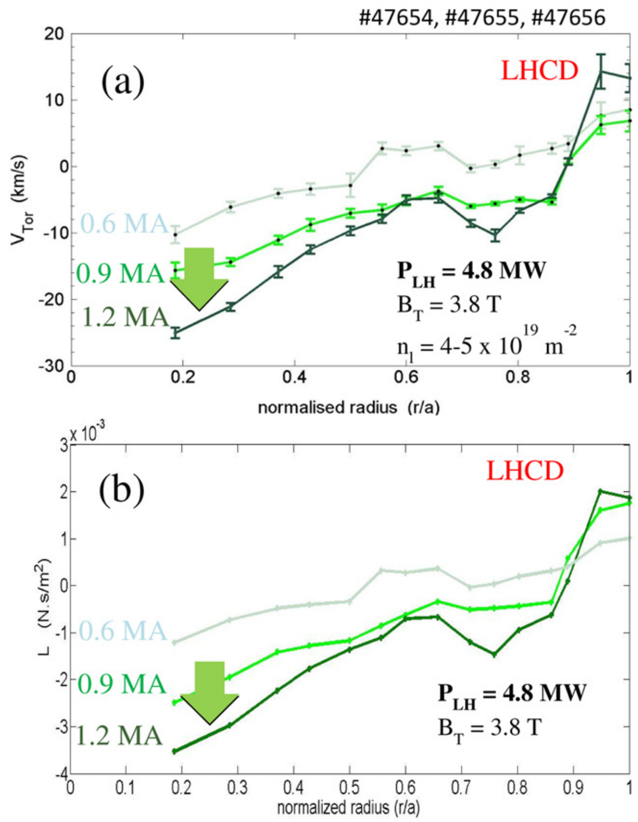


**Figure 7.** Toroidal rotation profile modifications with $I_p$ ($a$) and angular momentum profile evolution with $I_p$ ($b$) for LHCD plasmas.

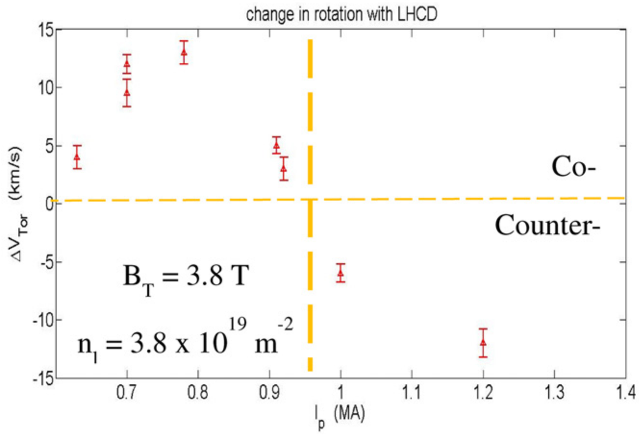


**Figure 8.** Evolution of the core rotation ($0.25 < r/a < 0.3$) change due to LHCD injection with plasma current. All data are at fixed density ($n_l = 3.8\times10^{19}\,\mathrm{m}^{-2}$). The vertical line indicates the zero crossing point, for which the plasma current is $I_{p,0} \sim 0.95\,\mathrm{MA}$.

currents as illustrated in figure 8, with $I_p = 0.6 - 1.22\,\mathrm{MA}$. It shows the change in the core rotation $\Delta V_\varphi$ (the velocity difference between the LHCD and OH plasmas) as a function of $I_p$, for plasma discharges with $B_T = 3.8\,\mathrm{T}$, $n_l \sim 3.8\times10^{19}\,\mathrm{m}^{-2}$ and $P_{LH} = 4.5\,\mathrm{MW}$. A zero crossing point in the plasma current amplitude is observed (referred as a stagnation point in [11]), the rotation increment switching from co- to counter-current direction when the plasma current increases. The observed zero crossing point (i.e. where the core rotation is not affected by LH injection, so that the velocity change is nearly zero) corresponds to $I_p \sim 0.95\,\mathrm{MA}$ for the presently discussed range of plasma parameters. As mentioned above, the sawtooth period is of about 30 ms at low $I_p$ (0.7 MA) and 50 ms at higher $I_p$ for OH plasmas. For the LHCD plasmas, the sawteeth are present only at high plasma current with a period between 30 and 60 ms.

## 4. Discussion of experimental observations and possible theoretical mechanisms

The experimental observations described above provide a rather clear picture of LH effects on plasma toroidal rotation in Tore Supra. Core plasma rotation observations at low plasma current are similar to those of C-Mod [11], JET [1], JT-60U [14] and EAST [12]. However, counter-current increments of plasma rotation (high plasma current case) have only been reported in C-Mod so far [10]. In C-Mod, the core velocity stagnation point is found at $I_p = 0.4\,\mathrm{MA}$, in lower single null plasmas (0.6 MA in upper single null configuration) and very different plasma conditions with $B_T = 5.4\,\mathrm{T}$, $n_e = 6.6\times10^{19}\,\mathrm{m}^{-3}$ and $P_{LH} = 0.8\,\mathrm{MW}$ [10]. According to C-Mod, the change in sign of the rotation increment could be consistent with a change in sign of the residual stress through its dependence on magnetic shear [9]. This could be the case in Tore Supra as well, although additional mechanisms could be taken into account as discussed below.

In Tore Supra OH plasmas, turbulence driven mechanisms and thermal ripple induced effects are at play. The latter drives momentum in the co/counter-current direction by creating a positive/negative radial electric field, hence causing rotation drive in the co/counter-current direction via the radial force balance. This effect increases linearly with the plasma current [31].

In LHCD plasmas, LH wave induced momentum and fast electron ripple loss effect add to the mechanisms listed above. The rotation ($|V_\varphi|$) increase with plasma current (see figure 7) seems consistent with momentum confinement improvement with $I_p$ [32]. Fast electron ripple losses induce a rotation increment in the co-current direction which increases with the plasma current [33]. Consequently momentum confinement improvement at higher $I_p$ seems to be the dominant mechanism in order to explain the experimental results. In all experimental cases reported above, turbulence driven mechanisms have also to be taken into account. One candidate could be related to plasma density gradient modification with $I_p$. When $I_p$ increases, the poloidal magnetic field $B_p \propto I_p/a$ increases in correlation with the plasma density gradient which favours the onset of radially localized modes, the frequency of which being proportional to the electron drift mode frequency (the collisionality being decreasing with $I_p$). This strong density gradient could induce ITG driven modes stabilization [32] and change the radial momentum transport. Whether such a momentum modification would lead to co- or counter-current rotation needs however to be investigated.

Significant theoretical effort is made to understand the LHCD induced rotation at low and high plasma currents. In Tore Supra LH heated discharges, the rotation behaviour likely results from the competition between several possible mechanisms at play as discussed above, as fast electron effects, turbulence driven mechanism effects, ripple-induced effects, MHD effects, and direct LH wave effects. In order to assess those effects, it is important to identify the different possible momenta acting on the toroidal rotation, and estimate their impact in the plasma. The toroidal momentum balance equation can be written as

$$n_s m_s \frac{\partial V_{s\varphi}}{\partial t} = e_s n_s E_\varphi - n_s m_s \nu_{ss'} \left(V_{s\varphi} - V_{s'\varphi}\right) + e_s \Gamma_{rs} B_\theta - \nabla \pi_{s\varphi} - \nabla \overline{\overline{\pi}}_\varphi + S, \quad (1)$$

where $s$ denotes the species, $V_{s\varphi}$ is the toroidal rotation of the considered species, $n_s$, $m_s$ the density and the mass of the particle, $e_s$ is the electron charge, $\nu_{ss'}$ is the collision frequency, $B_\theta$ is the poloidal magnetic field, $E_\varphi$ is the toroidal electric field, $\Gamma_{rs}$ the radial particle flux, $\nabla\overline{\overline{\pi}}_\varphi$ is the anisotropic part of the pressure tensor in the toroidal direction (viscosity tensor) and $\pi_{s\varphi} = -\chi_\varphi \nabla_r V_\varphi + \upsilon_\varphi V_\varphi + \pi_{\rm RS}$ is the toroidal tensor stress where $\chi_\varphi$ is the turbulent viscosity, $\upsilon_\varphi$ the velocity pinch and $\pi_{\rm RS}$ is the residual stress. In the right-hand side, the first term represents the Coulomb force, the second term the friction, the third one is the Laplace force and the last term is the sources. An estimation of the different terms is given for typical Tore Supra discharge.

The ripple-induced fast electron losses yield a return current directed outward, carried by ions, in order to maintain the ambipolarity condition. This return current induces a $J_{\rm ripple} \times B_\theta$ $(a)$ force in the co-current direction. However, experimental measurements of ripple loss current in Tore Supra [33] indicate that such a mechanism has an overall rather moderate effect ($M_{J_{\rm ripple} \times B} \approx 7 \times 10^{-3}\,{\rm N\,m^{-3}} \rightarrow \Delta V_\varphi \approx +5\,{\rm km\,s^{-1}}$). The particle ripple losses increase with the plasma current amplitude. According to the experimental results [33], fast electron ripple losses is larger than thermal electron ripple losses, hence cannot by itself explain the co-current increment observed at low $I_{\rm p}$. Another ripple-induced term contribution comes from the ripple-induced neoclassical friction associated to thermal particles following banana orbits. The friction acting on high energetic electrons is small because the collision frequency of ions with electrons decreases abruptly with the electron velocity [34] and could be determined by simulation. The thermal toroidal neoclassical friction can be written as $-n_s m_s \nu_{\rm neo}\left(V_{s\varphi} - k V_{\rm T}^*\right)$ with $\nu_{\rm neo}$ the neoclassical friction rate, $k$ a proportionality coefficient (detailed expressions can be found in [35, 36]) and $V_{\rm T}^* = \frac{\nabla_r T_{\rm i}}{e B_\theta}$ $(b)$ the toroidal diamagnetic velocity. For the plasma parameters considered in this chapter, the latter term can be responsible for a toroidal rotation increment in the counter-current direction of about $-10\,{\rm km\,s^{-1}}$ ($M_{\rm NF} \approx -13.2 \times 10^{-3}\,{\rm N\,m^{-3}} \rightarrow \Delta V_\varphi \approx -10\,{\rm km\,s^{-1}}$. The amplitude of this term evolves (increases) with plasma current amplitude and evolves also between the OH and the LHCD phases, via the ion temperature gradient (ITG). Ion temperature profiles for OH/LHCD plasmas, at low/high $I_{\rm p}$ are shown in figure 9. Regarding our experimental observations, it is clear than despite the strong ripple amplitude in Tore Supra, ripple induced effects cannot account for the various rotation behaviours. Another possible mechanism at play deals with momentum transfer between the LH waves and plasma electrons. The input torque from the LH wave can be estimated by the empirical formula used in [37]. This term leads to a change in the toroidal rotation directed in the counter-current direction of about $-3\,{\rm km\,s^{-1}}$ ($M_{\rm LH} \approx -4.1 \times 10^{-3}\,{\rm N\,m^{-3}} \rightarrow \Delta V_\varphi \approx -3\,{\rm km\,s^{-1}}$ which is weak but not negligible and likely does play a role in the resulting observed rotation. More accurate calculations have to be performed by LUKE simulations in order to confirm this source term effect. Moreover, turbulent transport processes $(d)$ can also drive angular momentum fluxes. In this case, the radial direction of the fluxes depends on the dominant turbulent modes present in the plasma, such as ITG or trapped electron mode (TEM). This mechanism depends on plasma current amplitude (high momentum confinement at high $I_{\rm p}$) and could partly explain the rotation increment reversal observed between low and high plasma current configurations. Different $q$-profiles are observed for low/high plasma current discharges as reported above. A change in the turbulent Reynolds stress, through a change in the residual stress (which depends on the plasma magnetic shear as detailed in [38]) or the pinch term, could also be considered as suggested in [9, 39]. Finally, the link between the observed rotation behaviour with LH heating and the presence or not of sawteeth is not obvious, and no clear correlation between the quantities associated with the sawteeth and the rotation profiles could be found. To summarize, the counter-current rotation profiles observed in OH and LHCD discharges could be mostly related to the neoclassical friction which induce a dominant counter-current rotation, even at low plasma current. Then, the impact of the LH power at low/high plasma current is due to the momentum transfer between LH waves and electrons, to the impact of $P_{\rm LH}$ and $I_{\rm p}$ on the neoclassical friction through the ITG, to the Laplace force through fast electron ripple losses and to the turbulent momentum fluxes as shown in [39]. The subtle combination of all terms cited above, illustrated in figure 10 could explain the co- or counter-current increment observed in the core toroidal plasma rotation. Those theoretical mechanisms with the support of quasi-linear gyro-kinetic simulations with QuaLiKiz [40], CRONOS and LUKE [41–43] are presently under investigation.

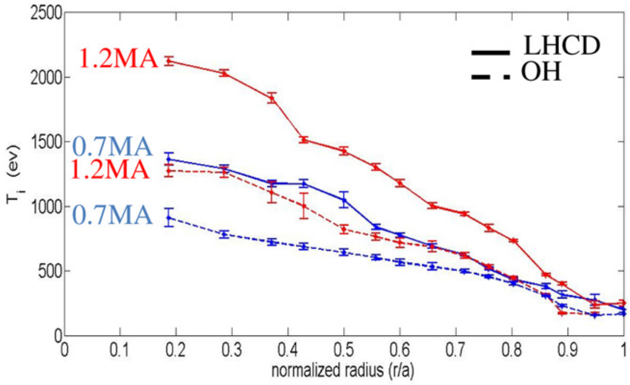


**Figure 9.** $T_{\rm i}$ profiles from CXRS measurements in OH (dashed curves) and LHCD (solid curves) plasmas for high and low plasma current discharges.

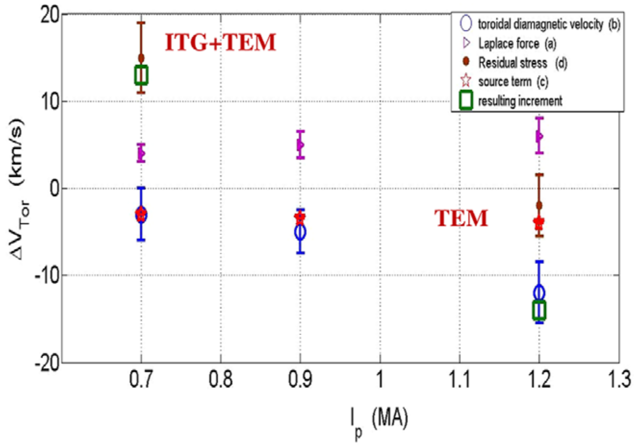


**Figure 10.** Typical contribution of the different mechanisms at play to the observed toroidal rotation, in terms of rotation increment in LHCD plasmas with $I_p = 0.7, 0.9, 1.2$ MA and $P_{LH} = 4.8$ MW: Laplace force (triangle symbols), ripple induced friction (circle symbols), residual stress (dot symbols, dominant term in the Reynolds stress inferred from TGLF [44] simulations), source term (star symbols) and the resulting increment (square symbols). As indicated by QuaLiKiz simulations, while ITG and TEM modes develop at low plasma current, at high plasma current only TEM modes are present.

## 5. Summary and conclusion

The lower hybrid heating and plasma current effects on plasma rotation have been investigated in a set of Tore Supra L-mode plasmas. We found that:

- The impact of lower hybrid heating on toroidal plasma rotation is correlated with the plasma current amplitude. At low plasma current ($I_p < 0.95$ MA) when the LH power is applied, the rotation change is in the co-current direction and impacts the whole rotation profile with an increment up to $+15\,\mathrm{km\,s^{-1}}$, increasing with the LH power magnitude. At higher plasma current, the toroidal rotation is affected in the core plasma region ($r/a < 0.6$) with an increment in the counter-current direction up to $-15\,\mathrm{km\,s^{-1}}$.
- Plasma rotation behaviour of an additional set of plasma discharges in LHCD scenario with similar LH power ($P_{LH} = 4.8$ MW) and $n_l$, but different $I_p$ amplitudes was investigated. The rotation increases in counter-current direction ($\Delta V_\varphi < 0$) when $I_p$ increases, in the bulk plasma region up to $r/a < 0.8$, with a maximum increment of about $-15\,\mathrm{km\,s^{-1}}$ in the core.
- A zero crossing point is identified at $I_p \sim 0.95$ MA for a given $P_{LH}$, where the resulting rotation is not affected by the LH power, that is also the point where the rotation change switches from co- to counter-current direction.

The rotation behaviour with LH heating results from a complex interaction of various mechanisms. The first analysis of the different terms contributing to the momentum balance equation shows that:

- The fast electron ripple loss mechanism leads to a co-current change in toroidal rotation.
- The thermal ripple induced neoclassical friction and absorbed LH momentum from LH waves via the resonant electrons is expected to influence the rotation in the counter-current direction,
- Depending on the turbulent modes (TEM, ITG) developed in the plasma, the radial turbulent transport can impact the rotation behaviour inducing increment in the co- or counter-current directions.
- The plasma current amplitude impacts all the above mechanisms except the LH source term where the $I_p$ amplitude effect on this term remains unclear. The neoclassical friction and the turbulent momentum transport (Reynolds stress) seem to be the dominant mechanisms to explain the LH heating induced rotation observed experimentally.

All those mechanisms will be discussed in details in a future paper.

## Acknowledgments

This work, supported by the European Communities under the contract of Association between EURATOM and CEA, was carried out within the framework of the European Fusion Development Agreement. The views and opinions expressed herein do not necessarily reflect those of the European Commission.

## References

[1] Burrell K H *et al* 1998 *Science* **281** 1816
[2] Garofalo A M *et al* 2001 *Nucl. Fusion* **41** 1171
[3] Doyle A M *et al* 2007 *Nucl. Fusion* **47** S18–127
[4] Lazzaro E *et al* 2002 Anomalous braking and shear modification of plasma rotation in a tokamak *Proc. 29th EPS Conf. (Montreux, Switzerland, 17–21 June 2002)* ECA vol 26B, pp P-5.079
[5] Eriksson L-G *et al* 2001 *Nucl. Fusion* **41** 91
[6] Stringer T E *et al* 1972 *Nucl. Fusion* **12** 689
[7] Yushmanov P N 1990 *Review of Plasma Physics* vol 16 (New York: Consultants Bureau)
[8] Podpaly Y A *et al* 2011 *PSFC/JA-11–30*
[9] Rice J *et al* 2013 Effects of magnetic shear on toroidal rotation in tokamak plasmas with lower hybrid current drive *Phys. Rev. Lett.* **111** 125003
[10] Rice J *et al* 2009 *Nucl. Fusion* **49** 025004
[11] Rice J E *et al* 2013 Effects of LHRF on toroidal rotation in Alcator C-Mod plasmas *Nucl. Fusion* **53** 093015
[12] Shi Y *et al* 2011 *Phys. Rev. Lett.* **106** 235001
[13] Eriksson L-G *et al* 2009 *Plasma Phys. Control. Fusion* **51** 044008
[14] Sakamoto Y *et al* 2006 *Plasma Phys. Control. Fusion* **48** A63
[15] Platz P *et al* 1995 *22nd European Physical Society Conf. on Plasma Physics and Controlled Fusion (Bournemouth, UK, 1995)* vol 19C, Part III-337
[16] Fenzi C *et al* 2011 Toroidal magnetic field ripple and fast particle effects on plasma rotation in Tore Supra *Proc. 32nd EPS Conf. on Plasma Physics (Strasbourg, 27 June–July 2011)*
[17] Segui J L *et al* 2005 *Rev. Sci. Instrum.* **76** 123501
[18] Clairet F *et al* 2010 *Rev. Sci. Instrum.* **81** 10D903
[19] Gil C *et al* 2009 *Fusion Sci. Technol.* **56** 1219
[20] Basiuk V *et al* 1995 *Nucl. Fusion* **35** 12
[21] Artaud J-F *et al* 2010 *Nucl. Fusion* **50** 043001

[22] Fenzi C *et al* 2011 *Nucl. Fusion* **51** 103038
[23] Grierson B A *et al* 2012 Measurements of the deuterium ion toroidal rotation in the DIII-D tokamak and comparison to neoclassical theory *Phys. Plasmas* **19** 056107
[24] Testa D *et al* 2002 On the measurement of toroidal rotation for the impurity and the main ion species on the Joint European Torus *Phys. Plasmas* **9**
[25] von Hellerman M G 2007 *CXSFIT User Manual*
[26] Guilhem D *et al* 2009 Passive active multi-junction 3.7 GHz launcher for Tore-Supra long pulse experiments: manufacturing process and tests *Proc. 18th Topical Conf. on Radio Frequency Power in Plasmas, AIP Conf. Proc. (Gent, Belgium, June 2009)* **1187** 435–8
[27] van Houtte D *et al* 2004 *Nucl. Fusion* **44** L11
[28] Peysson Y *et al* 2000 *Plasma Phys. Control. Fusion* **42** B87
[29] Imbeaux F *et al* 2005 Ray-tracing and Fokker–Planck modelling of the effect of plasma current on the absorption and propagation of lower hybrid waves *Plasma Phys. Control. Fusion* **47** 2041–65
[30] Nilsson E *et al* 2013 Comparative modelling of lower hybrid current drive with two launcher designs in the Tore Supra tokamak *Nucl. Fusion* **53** 083018
[31] Peysson Y *et al* 1996 *Phys. Plasmas* **3** 3668
[32] Fukuyama A *et al* 1995 Transport simulation on L-mode and improved confinement associated with current profile modification *Plasma Phys. Control. Fusion* **37** 611431
[33] Basiuk V *et al* 2001 *Nucl. Fusion* **5** 41
[34] Gurevicha A 1978 Kinetic theory of runaway production in toroidal magnetic devices *Nucl. Fusion* **18** 5
[35] Fenzi C *et al* 2011 On plasma rotation with toroidal magnetic field ripple and no external momentum input *Nucl. Fusion* **51** 103038
[36] Garbet X *et al* 2010 *Phys. Plasmas* **17** 072505
[37] Eriksson L-G *et al* 2010 *Plasma Phys. Control. Fusion* **51** 044008
[38] Wang L and Diamond P H 2013 Gyrokinetic theory of turbulent acceleration of parallel rotation in tokamak plasmas *Phys. Rev. Lett.* **110** 265006
[39] Kluy N *et al* 2009 Linear gyrokinetic calculations of toroidal momentum transport in the presence of trapped electron modes in tokamak plasmas *Phys. Plasmas* **16** 122302
[40] Bourdelle C *et al* 2007 *Phys. Plasmas* **14** 112501
[41] Decker Y P J 2004 A fast numerical solver for the 3D drift kinetic equation *Report* EUR-CEA-FC-1736, Euratom-CEA
[42] Peysson Y and Decker J 2014 *Fusion Sci. Technol.* **65**
[43] Peysson Y, Decker J and Morini L 2012 *Plasma Phys. Control. Fusion* **54** 045003
[44] Staebler G M, Waltz R E, Candy J and Kinsey J E 2013 *Phys. Rev. Lett.* **110** 055003